Non-linear Model Predictive Control of Cabin Temperature and Air Quality in Fully Electric Vehicles

Jan Glos, Lukáš Otava, Pavel Václavek

Accepted manuscript

J. Glos, L. Otava and P. Václavek, "Non-Linear Model Predictive Control of Cabin Temperature and Air Quality in Fully Electric Vehicles," in IEEE Transactions on Vehicular Technology, vol. 70, no. 2, pp. 1216-1229, Feb. 2021, doi: 10.1109/TVT.2021.3054170.

DOI: 10.1109/TVT.2021.3054170

IEEE Xplore: ieeexplore.ieee.org

Non-linear Model Predictive Control of Cabin Temperature and Air Quality in Fully Electric Vehicles

Jan Glos, Lukáš Otava, Pavel Václavek, *Senior Member, IEEE*

***Abstract*—This article describes an application of Non-linear Model Predictive Control algorithms on energy efficient control of fully electric vehicle cabin temperature and air quality. Since fully electric vehicles can not utilize waste heat from a powertrain (or there is not enough waste heat) as ICE vehicles do, it is necessary to employ advanced control approaches (especially for cabin heating) due to the possible mileage lost by using energy from the batteries for cabin conditioning. The basic idea behind this is to avoid the heat losses caused by excessive air exchange and to ensure a satisfactory air quality in combination with a user defined temperature. The Non-linear Model Predictive control algorithms were successfully implemented into an Infineon AURIX Tricore microcontroller and tested within a Processor in the Loop simulation.**

***Index Terms*—non-linear model predictive control, fully electric vehicle, battery electric vehicle, vehicle cabin model, Extended Kalman filter, air quality control, temperature control**

NOMENCLATURE

COP	Coefficient of Performance
EKF	Extended Kalman Filter
EV	Electric Vehicle
FEV	Fully Electric Vehicle
FMU	Functional Mockup Unit
HVAC	Heating, Ventilation, and Air Conditioning
HX	Heat Exchanger
ICE	Internal Combustion Engine
ISR	Interrupt Service Routine
MCU	Microcontroller unit
MIL	Model in the Loop
MPC	Model Predictive Control
NMPC	Non-linear Model Predictive Control
OCP	Optimal Control Problem
PHEV	Plug-in Hybrid Electric Vehicle
PIL	Processor in the Loop
PTC	Positive Temperature Coefficient (heater)
SIL	Software in the Loop

c	Specific heat capacity
C	Heat capacity
f	Frequency
G	Thermal conductance
$\mathbf{H}$	State-space representation output matrix
I	Electric current
$\dot{m}$	Mass flow rate
P	Power consumption
Q	Heat
$\dot{Q}$	Heat flow rate
$\mathbf{Q}$	Weighting matrix
$\mathbf{r}$	State-space representation references vector
T	Temperature
$\mathbf{u}$	State-space representation input vector
U	Voltage
V	Volume
$\dot{V}$	Volume flow rate
W	Work
$\mathbf{x}$	State-space representation state vector
$\mathbf{z}$	State-space representation output vector
ρ	Volumetric mass density
κ	Air quality

Manuscript received XXX, XX, 2020; revised XXX, XX, 2020.

The authors are with CEITEC - Central European Institute of Technology, Brno University of Technology, Brno, Czech Republic. Pavel Václavek is also with the Faculty of Electrical Engineering and Communication, Brno University of Technology, Brno, Czech Republic. (e-mail: jan.glos@vut.cz, lukas.otava@ceitec.vutbr.cz, pavel.vaclavek@ceitec.vutbr.cz)

I. INTRODUCTION

Fully electric vehicles (FEV) require special approaches for cabin heating, as the classical solution adapted from internal combustion engine (ICE) vehicles is not satisfactory from the perspective of energy consumption. ICE vehicles utilize waste heat from the ICE for cabin heating. The ICE's tank-to-wheel efficiency is usually $20\,\%$ to $40\,\%$, and approximately $30\,\%$ of total energy can be used for cabin heating [1]–[3]. If we consider a petrol ICE, the energy density is $34.2\,\mathrm{MJ\,l^{-1}}$. For city driving with an average speed of $40\,\mathrm{km\,h^{-1}}$ and an average fuel consumption of $8\,\mathrm{l}/100\mathrm{km}$, there is an available thermal flow of $9\,\mathrm{kW}$ on average for cabin heating.

On the other hand, the electric vehicle (EV) powertrain has a much higher overall efficiency ($67\,\%$ to $82\,\%$), with approx. $10\,\%$ to $25\,\%$ converted to waste heat [4]. As a result, the EV generates a maximum waste heat flow rate of approx. $0.85\,\mathrm{kW}$ to $2\,\mathrm{kW}$ under the same conditions as for the ICE vehicle above. Moreover, part of this thermal flow is from a low potential source, as the batteries temperature can not be higher than approx. $30\,^{\circ}\mathrm{C}$ to $40\,^{\circ}\mathrm{C}$. Thus, the coolant temperature will be even lower and the use for cabin heating is quite complicated. The waste heat recovery makes sense in

combination with the use of a heat pump system, which would elevate the temperature for cabin heating.

It needs to be mentioned that waste heat recovery for EVs is not state-of-the-art technology, and there is no common understanding among the manufacturers. Current EVs use positive temperature coefficient (PTC) heaters, air to water heat pumps, or their combination, as a heat source [5].

Regardless of the heat source, a cabin heating system needs to be powered from batteries and the power consumption negatively influences the mileage of the EV. An extremely unpleasant choice can occur when the user needs to decide if the EV will heat the cabin or reach its destination.

This paper proposes a partial solution to this problem. The basic goal is to keep the range of the EV as long as possible, which means minimizing the energy needed for cabin heating. This target can be achieved by multiple methods, and preferably by their combination

- minimizing the cabin thermal losses through walls and windows (insulation etc.)
- minimizing the thermal losses through cabin ventilation
- improvement of the heat source (e.g. from a PTC heater with a coefficient of performance (COP) of 1.0, to a heat pump with a COP of 1.5 to 3)
- waste heat recovery from the electric motor, power electronics and battery
- utilization of thermal energy storage (based on phase-change material)

This work is focused on the second bullet point, and brings an increased range to the EV by minimizing the heat losses through ventilation, using advanced control of the cabin heating actuators.

The other bullet points require complex changes to a vehicle, especially in mechanical design, obviously with influence on the electrical system, thermal management system and also the control algorithms. However, the benefits of proper ventilation and the heating control approach should be the highest (compared to other methods, where the major benefits mostly come from proper design), so the paper is focused on this method.

It is obvious that with full cabin air recirculation, minimal heat requirements would be achieved. Nevertheless, this approach can not be used, as no fresh air will be supplied to the cabin and thus the air quality will be deteriorated by means of a higher carbon dioxide (CO_2) concentration. High concentrations of CO_2 can lead to driver (and also passenger) fatigue [6]. Moreover, the cabin air humidity can increase and under some conditions windows can get fogged, leading to a limited driver view. Both these problems can negatively influence the driver comfort and attention, which could in the worst case cause an accident.

In this article, the C-segment passenger car (or its equivalent, like the US compact car) is considered to have a cabin compartment volume of $3000\,\mathrm{l}$ and length of approx. $4.5\,\mathrm{m}$.

As a first preview to the required thermal flows for vehicle cabin heating, we performed a set of simulations, whose results are presented in Fig. 1 and 2. We evaluate the results using three variables. First, κ stands for the cabin air quality, which is dependent on HVAC fan speed and fresh air flap setting.

TABLE I: Actuators and conditions for basic cabin thermal flow simulations

Actuator/condition name	Symbol	Value
Coolant mass flow rate	$\dot{m}_{\mathrm{h5}}$	$0.4\,\mathrm{kg\,s^{-1}}$
Air mass flow rate	$\dot{m}_{\mathrm{c}}$	$0.07\,\mathrm{kg\,s^{-1}}$
Thermal flow to coolant	$\dot{Q}_{\mathrm{h10}}$	dependent
Fresh air flap	φ	independent
Cabin air quality	κ	dependent
Number of passengers	n_{pas}	2
Ambient temperature	T_{c5}	$-10\,^{\circ}\mathrm{C}$
Cabin temperature reference	T_{c1}	$20\,^{\circ}\mathrm{C}$

The second and third variables are used to measure the heat supplied into the cabin (which needs to be generated from electric energy in batteries by a heat pump or PTC and thus affects the EV range). We use a heat requirement Q as a variable describing total thermal energy provided into the cabin during some period (30-minute drive including heat build-up in Fig. 1). Then we use variable heat flow rate $\dot{Q}$ to show the instantaneous steady-state heating power required to compensate the thermal losses of the cabin with keeping the cabin temperature at the defined reference temperature. The simulations were executed in Dymola, based on the model described in section II-E, with constant controls (apart from the heat source and fresh air flap) and ambient conditions, defined in Table I.

In Fig. 1, there is the heat required for cabin heat build-up during a 30 minute drive presented. All the vehicle parts were initially at the ambient temperature and then we started heating up the cabin, and this process was repeated for different settings of the fresh air flap $\varphi \in \{0, 10, 25, 50, 75, 100\}\ (\%)$. This setting was kept constant during the individual simulation runs and the results for the dependent variables of all the runs are shown in Fig. 1. It is evident that both the required heat and the resulting cabin air quality are strongly dependent on the fresh air flap setting. Then, two important conclusions can be obtained from Fig. 1:

1) The fresh air flap - needs to be kept above approx. $25\,\%$ to achieve satisfactory cabin air quality ($\kappa \approx 1000\,\mathrm{ppm}$; considering 2 passengers and $\dot{m}_{\mathrm{c}} = 0.07\,\mathrm{kg\,s^{-1}}$; with possible short-term lower values of the fresh air ratio)
2) A heat source in the order of kW (e.g. $4\,\mathrm{kW}$ to $8\,\mathrm{kW}$) is needed for cabin heat build-up (note: even all the waste heat from an EV powertrain is not sufficient).

Then we introduce Fig. 2, which presents the steady-state heat flow rate dependency on the fresh air flap setting. It is evident that the fresh air flap can not be entirely closed (full recirculation) and that the heat flow rate is highly dependent on its value.

Regarding the influence of cabin heating on vehicle range, in the worst case (under conditions defined in Tab. I), the heat source would consume approx. $2.3\,\mathrm{kW\,h}$ per cabin heat build-up and $3\,\mathrm{kW\,h}$ per each hour of driving, with a higher air mass flow rate the power consumption would be also higher. For a mid-size EV (such as a Mercedes B, Nissan Leaf) that means

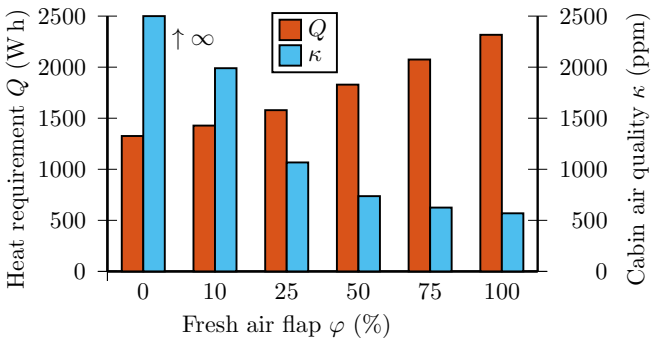

Fig. 1: Heat required by a heating system for cabin heat build-up during a 30 minute drive (conditions defined in Tab. I)

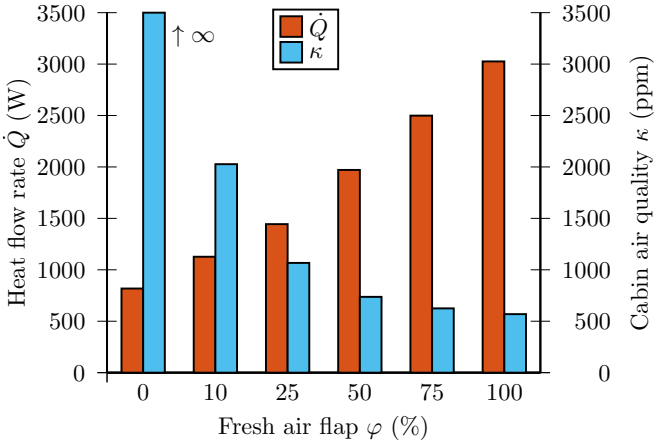

Fig. 2: Heat flow rate needed for cabin heating in a steady state (conditions defined in Tab. I)

a loss of mileage by $7.6\,\%$ due to cabin heat build-up and $10\,\%$ per each hour of operation. This model case didn't take into account the power consumption of the fan and coolant pump, a possible lower ambient temperature, heat losses in the engine compartment, and other influences that might make the range loss even higher. The conclusion from this analysis is that cabin heating can have a strong negative influence on EV range.

At this point, we should summarize the requirements on cabin environment control:

1) Temperature - keep it at a (user) defined reference
2) Air quality - keep it at a reasonable value (approx. $600\,\mathrm{ppm}$ to $1000\,\mathrm{ppm}$, short time up to $1500\,\mathrm{ppm}$)
3) Power consumption - minimize power of the heat source, fan and coolant pump
4) Noise - keep the fan speed as low as possible

The controlled system control inputs are constrained, moreover, its internal states and outputs are constrained too (e.g. supply air temperature should not exceed $60\,^{\circ}\mathrm{C}$, coolant temperature $90\,^{\circ}\mathrm{C}$, etc.).

Considering the above requirements, one of the preferable control approaches is Non-linear Model Predictive Control (NMPC). The traditional control approaches introduce a high number of additional control references, switching between control scenarios (e.g. heat build-up, steady-state, etc.), and complicated state constraints compliance. Moreover, the system has four inputs, two outputs, significant cross-couplings between inputs, and outputs and power consumption optimization is required. In the end, the traditional control system would become overcomplicated, thus the NMPC approach is preferable from our perspective.

Cabin thermal management algorithms using NMPC and linear-quadratic strategy were proposed in [7], where the authors assembled vehicle cabin and HVAC model (including humidity and carbon dioxide concentration), which they then used for algorithms design and verification by simulation. Model predictive control combined with the neural network was used in [8] for automotive compressor speed control and their solution brings substantial improvement of cabin temperature reference tracking and disturbance rejection. A hierarchical MPC scheme was proposed for combined cabin and battery thermal management in [9]. Their approach can cover different dynamics (relatively fast and slow) in the vehicle thermal management system. MPC combined with different forecast methods of passenger number was prepared in [10] for cabin temperature control of an electric bus. The Markov-chain based prediction gave them the lowest energy consumption of the HVAC system. Nonlinear model predictive control was used in [11] for vehicle cabin temperature control with evaporator temperature setpoint and blower speed as controlled variables.

NMPC applied on Plug-in Hybrid Electric Vehicle (PHEV) thermal management (battery, charger and power electronics cooling) was successfully tested in a Software in the Loop (SIL) simulation [12] and then tested in the real environment [13]. Model predictive on-off control for cabin heating in ICE vehicles was developed and implemented in [14]. The HVAC system, including the heat pump, was successfully controlled by NMPC in [15] with NMPC running on an Intel i5 $2.6\,\mathrm{GHz}$ quadcore processor of a laptop. The model of the automotive air-conditioning/refrigeration system with cargo was assembled in [16] and the authors showed that several different types of MPC controllers provide substantially better performance (in terms of power consumption and cargo temperature reference tracking) compared to the on/off controller. There are also several papers on cabin air quality and ventilation, such as [17], [18], but none of them links the air quality with power consumption for heating. The indoor air quality control is quite often used in building environment control, in combination with MPC, reported, for example by [19]. The authors of [20] proposed linear MPC for vehicle cabin heating, and in conclusion they call for considering cabin air recirculation in an MPC control strategy.

Model predictive control is also widely used in different automotive applications, especially for fuel consumption reduction [21]–[24], path tracking [25], [26] and cruise control [27]–[29].

As far as we at best know, there is no implementation of NMPC in an automotive grade processor in series production for EV cabin heating with respect to cabin air quality.

II. FEV HVAC DYNAMIC MODELS

A vehicle cabin (complemented with an HVAC system) is quite complicated to be modelled from a thermal point of view. It consists of a high number of materials, including both the thermal insulants (foam, plastics etc.) and thermal conductors (metal, glass, etc.). There are also a lot of other influences on cabin thermal behaviour, such as the radiative thermal flow from the sun, passenger thermal flow, forced convection during driving, ventilation using windows, etc.

Thus, the model describing all the above mentioned effects, and reflecting all the heat transfer types (like Dymola reference model in Subsection II-E), would be very complicated and not useful for NMPC design. Therefore, the structure of the model was simplified to represent a grey box model, where the structure is fixed and the parameters are guessed, or identified, and can be considered as lumped (e.g. the thermal flow through the cabin walls are represented by single thermal conductance G_{c1}, which has no representation in a real system, but is used as a cumulative variable).

A. HVAC Thermal Model

The simplified HVAC system in Fig. 3 can be described by the following set of equations

$$C_{\mathrm{h1}}\frac{\mathrm{d}T_{\mathrm{h1}}}{\mathrm{d}t} = \dot{Q}_{\mathrm{h7}} + \dot{Q}_{\mathrm{h5}} - \dot{Q}_{\mathrm{h6}}, \tag{1}$$

$$C_{\mathrm{h3}}\frac{\mathrm{d}T_{\mathrm{h3}}}{\mathrm{d}t} = \dot{Q}_{\mathrm{h9}} - \dot{Q}_{\mathrm{h8}} - \dot{Q}_{\mathrm{h7}}, \tag{2}$$

$$C_{\mathrm{h4}}\frac{\mathrm{d}T_{\mathrm{h4}}}{\mathrm{d}t} = \dot{Q}_{\mathrm{h8}} - \dot{Q}_{\mathrm{h9}} + \dot{Q}_{\mathrm{h10}}, \tag{3}$$

where C denotes thermal capacity, T stands for thermodynamic temperature, and $\dot{Q}$ is a general thermal flow rate.

Heat exchanger 1 (HX1) is used as a condenser and the refrigerant is rejecting heat into the coolant with a temperature of T_{h4}, and it is circulated by the coolant pump (P1). HX1 and the heat flow rate $\dot{Q}_{\mathrm{h10}}$ could be replaced by another heat source (PTC, etc.) for a different application. The air is heated by the coolant in HX2 and then supplied to the vehicle cabin. The temperature of the cooled coolant at the HX2 outlet is denoted as T_{h3} and T_{h1} stands for a temperature of heated air. The air from the cabin (with a temperature of T_{c1}) can be exhausted outside or reused by operating a fresh air flap. The fresh air flap mixes the recirculated air from the cabin with the fresh air of temperature T_{h5} and the resulting air temperature at the flap outlet is marked as T_{h2}. The air movement is assured by the HVAC fan (F1).

We assume that the fan and pump speeds can be controlled and the heat flow rate $\dot{Q}_{\mathrm{h10}}$ can be adjusted by compressor speed control (or, in general, by heat source control for a Positive Temperature Coefficient (PTC) heater, etc.).

The heat flow rates from Fig. 3 can be expressed as

$$\dot{Q}_{\mathrm{h5}} = \dot{m}_{\mathrm{h1}} c_{\mathrm{h}} T_{\mathrm{h2}}, \tag{4}$$

$$\dot{Q}_{\mathrm{h6}} = \dot{m}_{\mathrm{h1}} c_{\mathrm{h}} T_{\mathrm{h1}}, \tag{5}$$

$$\dot{Q}_{\mathrm{h7}} = G_{\mathrm{h7}}(T_{\mathrm{h3}} - T_{\mathrm{h1}}), \tag{6}$$

$$\dot{Q}_{\mathrm{h8}} = \dot{m}_{\mathrm{h5}} c_{\mathrm{co}} T_{\mathrm{h3}}, \tag{7}$$

$$\dot{Q}_{\mathrm{h9}} = \dot{m}_{\mathrm{h5}} c_{\mathrm{co}} T_{\mathrm{h4}}. \tag{8}$$

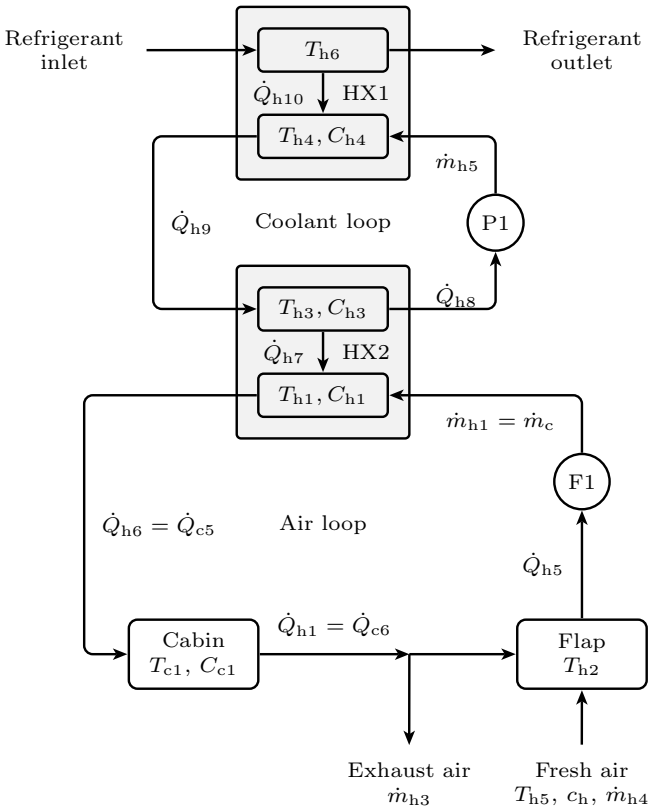

Fig. 3: FEV HVAC model

The heat flow rate between the coolant and the air in the HX2 is described by (6), what is the most simple expression of heat exchanger thermal flow rate, which is dependent on media temperatures and thermal conductance G_{h7}. The rest of the equations above are based on the Simplified Steady-Flow Energy Equation (SSFEE) from [30]. In the equations, $\dot{m}_{\mathrm{h1}}$ stands for the air mass flow rate caused by the HVAC fan, c_{h} is the air specific thermal capacity, $\dot{m}_{\mathrm{h5}}$ is the coolant mass flow rate caused by the coolant pump, and c_{co} is the coolant specific thermal capacity.

After substitution of (4-8) to (1-3), and minor modifications, a new set of equations can be obtained

$$\frac{\mathrm{d}T_{\mathrm{h1}}}{\mathrm{d}t} = \frac{1}{C_{\mathrm{h1}}}[G_{\mathrm{h7}}(T_{\mathrm{h3}} - T_{\mathrm{h1}}) + \dot{m}_{\mathrm{h1}} c_{\mathrm{h}}(T_{\mathrm{h2}} - T_{\mathrm{h1}})], \tag{9}$$

$$\frac{\mathrm{d}T_{\mathrm{h3}}}{\mathrm{d}t} = \frac{1}{C_{\mathrm{h3}}}[\dot{m}_{\mathrm{h5}} c_{\mathrm{co}}(T_{\mathrm{h4}} - T_{\mathrm{h3}}) - G_{\mathrm{h7}}(T_{\mathrm{h3}} - T_{\mathrm{h1}})], \tag{10}$$

$$\frac{\mathrm{d}T_{\mathrm{h4}}}{\mathrm{d}t} = \frac{1}{C_{\mathrm{h4}}}[\dot{m}_{\mathrm{h5}} c_{\mathrm{co}}(T_{\mathrm{h3}} - T_{\mathrm{h4}}) + \dot{Q}_{\mathrm{h10}}], \tag{11}$$

$$T_{\mathrm{h2}} = \varphi T_{\mathrm{h5}} + (1 - \varphi) T_{\mathrm{c1}}, \tag{12}$$

where φ is the fresh air flap status (0 to 1) and it is used for mixing the fresh and recirculated air and computing the resulting temperature.

The cabin model (represented by a block in the lower-left corner in Fig. 3) is described in detail in the following section.

B. Cabin Thermal Model

The cabin model overview can be found in Fig. 4. The model can be in general described by the following equations

$$C_{\mathrm{c1}}\frac{\mathrm{d}T_{\mathrm{c1}}}{\mathrm{d}t} = \dot{Q}_{\mathrm{c1}} + \dot{Q}_{\mathrm{c2}} + \dot{Q}_{\mathrm{c5}} + \dot{Q}_{\mathrm{c4}} + \dot{Q}_{\mathrm{c3}} - \dot{Q}_{\mathrm{c6}}, \quad (13)$$

$$C_{\mathrm{c2}}\frac{\mathrm{d}T_{\mathrm{c2}}}{\mathrm{d}t} = -\dot{Q}_{\mathrm{c3}}, \quad (14)$$

$$C_{\mathrm{c3}}\frac{\mathrm{d}T_{\mathrm{c3}}}{\mathrm{d}t} = -\dot{Q}_{\mathrm{c1}} + \dot{Q}_{\mathrm{c7}} + \dot{Q}_{\mathrm{c8}}, \quad (15)$$

$$C_{\mathrm{c4}}\frac{\mathrm{d}T_{\mathrm{c4}}}{\mathrm{d}t} = -\dot{Q}_{\mathrm{c2}} + \dot{Q}_{\mathrm{c9}}, \quad (16)$$

where T_{c1} is the cabin air temperature, T_{c2} stands for a temperature of the cabin equipment (seats, dashboard, etc.), T_{c3} is the temperature of the cabin walls, and T_{c4} is the temperature of the windows. The thermal capacities C_{cx} are indexed in the same manner as the temperatures.

The equations above can be then modified to the substituted form

$$\frac{\mathrm{d}T_{\mathrm{c1}}}{\mathrm{d}t} = \frac{1}{C_{\mathrm{c1}}}[G_{\mathrm{c1}}(T_{\mathrm{c3}} - T_{\mathrm{c1}}) + G_{\mathrm{c2}}(T_{\mathrm{c4}} - T_{\mathrm{c1}}) + \dot{m}_{\mathrm{c}}c_{\mathrm{c}}(T_{\mathrm{h1}} - T_{\mathrm{c1}}) + \dot{Q}_{\mathrm{c4}} + G_{\mathrm{c3}}(T_{\mathrm{c2}} - T_{\mathrm{c1}})], \quad (17)$$

$$\frac{\mathrm{d}T_{\mathrm{c2}}}{\mathrm{d}t} = \frac{1}{C_{\mathrm{c2}}}[-G_{\mathrm{c3}}(T_{\mathrm{c2}} - T_{\mathrm{c1}})], \quad (18)$$

$$\frac{\mathrm{d}T_{\mathrm{c3}}}{\mathrm{d}t} = \frac{1}{C_{\mathrm{c3}}}[-G_{\mathrm{c1}}(T_{\mathrm{c3}} - T_{\mathrm{c1}}) + \dot{Q}_{\mathrm{c7}} + G_{\mathrm{c8}}(T_{\mathrm{c5}} - T_{\mathrm{c3}})], \quad (19)$$

$$\frac{\mathrm{d}T_{\mathrm{c4}}}{\mathrm{d}t} = \frac{1}{C_{\mathrm{c4}}}[-G_{\mathrm{c2}}(T_{\mathrm{c4}} - T_{\mathrm{c1}}) + G_{\mathrm{c9}}(T_{\mathrm{c5}} - T_{\mathrm{c4}})], \quad (20)$$

where $\dot{m}_{\mathrm{c}} = \dot{m}_{\mathrm{h1}}$ and stands for the air mass flow rate through the cabin (caused by the HVAC fan), $c_{\mathrm{c}} = c_{\mathrm{h}}$ and is the air specific thermal capacity, $\dot{Q}_{\mathrm{c7}}$ is the solar heat flow rate and $\dot{Q}_{\mathrm{c4}}$ is the passenger heat flow rate. The cabin air inlet and outlet is described by $\dot{Q}_{\mathrm{c5}}$ and $\dot{Q}_{\mathrm{c5}}$, respectively, and then expressed using SSFEE (similarly as for HVAC model). The rest of the heat flow rates represent conductive, convective, and radiative thermal transfers between the cabin parts. For simplicity of the model, all the heat transfer types between two parts are aggregated into a single equation term, which is dependent on part's temperatures and associated thermal conductance G_{cx}, where the index corresponds to the general heat flow rate index ($\dot{Q}_{\mathrm{cx}}$). The thermal conductances are generalized constants, which were identified and have no physical representation (can not be computed based on part materials and dimensions).

C. Cabin air quality model

We can define the air quality in the most used form [31], i.e. as a ratio of CO_2 to the whole (cabin or any unit). The air quality can be expressed in percent or in ppm (commonly used for indoor air quality evaluation [31], [32]).

The air quality model we developed consists of two components - human respiration and HVAC air exchange. The first component is modelled based on the fact, that during every inhale some amount of the air (of cabin air quality) is removed from the cabin and during the exhale, the same amount of the air (of deteriorated quality) is returned into the cabin. The second component describes the ventilation of the cabin similarly - HVAC air volume flow rate brings and takes away the air of different quality. Moreover, the ventilation performance is controlled by the fresh air flap.

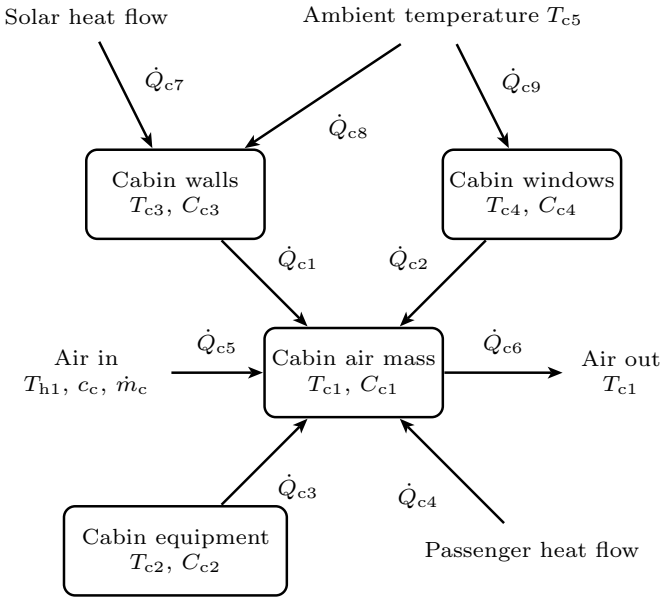

Fig. 4: FEV cabin thermal model

The behaviour of air quality inside a vehicle cabin can be described by

$$V\frac{\mathrm{d}\kappa}{\mathrm{d}t} = n_{\mathrm{pas}}\dot{V}_{\mathrm{res}}(\kappa_{\mathrm{ex}} - \kappa) + \varphi\dot{V}_{\mathrm{HVAC}}(\kappa_{\mathrm{amb}} - \kappa), \quad (21)$$

where κ is cabin air quality, κ_{ex} the exhaled air quality, κ_{amb} the ambient air quality, $\dot{V}_{\mathrm{res}}$ is respiratory volume flow rate, $\dot{V}_{\mathrm{HVAC}}$ the volume flow rate of the HVAC, n_{pas} is the number of passengers in the vehicle, φ is the fresh air flap state ($\varphi = 1$: only fresh air, $\varphi = 0$: only recirculated air) and V is the cabin volume.

Respiratory volume flow rate can be computed as

$$\dot{V}_{\mathrm{res}} = f_{\mathrm{res}}V_{\mathrm{res}}, \quad (22)$$

where $f_{\mathrm{res}} = 0.25\,\mathrm{Hz}$ is respiratory frequency and $V_{\mathrm{res}} = 0.0005\,\mathrm{m}^3$ is respiratory volume [33], which leads to

$$\frac{\mathrm{d}\kappa}{\mathrm{d}t} = \frac{1}{V}\left[n_{\mathrm{pas}}f_{\mathrm{res}}V_{\mathrm{res}}(\kappa_{\mathrm{ex}} - \kappa) + \varphi\frac{\dot{m}_{\mathrm{c}}}{\rho_{\mathrm{c}}}(\kappa_{\mathrm{amb}} - \kappa)\right], \quad (23)$$

where $\dot{m}_{\mathrm{c}}$ is the air mass flow rate defined in Subsection II-B and ρ_{c} stands for cabin air mass density.

D. Overall cabin and HVAC model

The resulting dynamic model of the FEV cabin and HVAC was prepared as a combination of the equations above

$$\dot{\mathbf{x}} = \mathbf{f}(\mathbf{x}, \mathbf{u}), \quad (24)$$

$$\mathbf{z} = \mathbf{h}(\mathbf{x}), \quad (25)$$

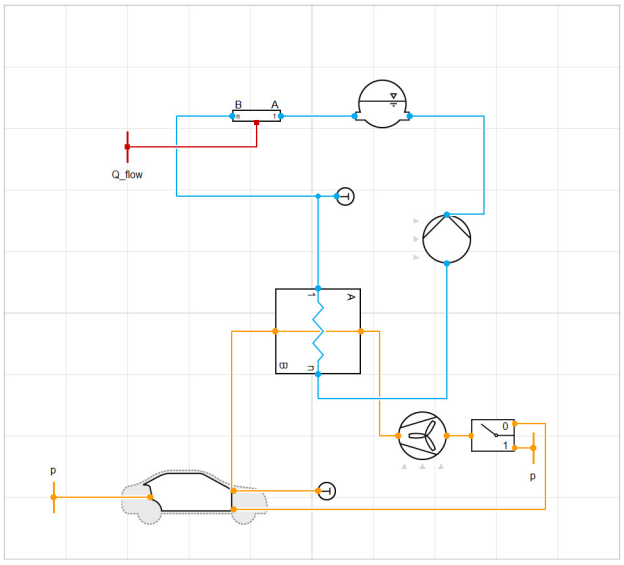

Fig. 5: Reference model of the cabin and HVAC in Dymola

with state ($\mathbf{x}$), input ($\mathbf{u}$) and output ($\mathbf{z}$) vectors

$$\begin{aligned}\mathbf{x} &= \begin{bmatrix} T_{\mathrm{c1}} & T_{\mathrm{c2}} & T_{\mathrm{c3}} & T_{\mathrm{c4}} & T_{\mathrm{h1}} & T_{\mathrm{h3}} & T_{\mathrm{h4}} & \kappa \end{bmatrix}^{\mathsf{T}}, \\ \mathbf{u} &= \begin{bmatrix} \dot{m}_{\mathrm{h5}} & \dot{m}_{\mathrm{c}} & \dot{Q}_{\mathrm{h10}} & \varphi \end{bmatrix}^{\mathsf{T}}, \\ \mathbf{z} &= \begin{bmatrix} z_{T_{\mathrm{c1}}} & z_{T_{\mathrm{h1}}} & z_{T_{\mathrm{h4}}} & z_{\kappa} \end{bmatrix}^{\mathsf{T}}, \end{aligned} \tag{26}$$

and $\mathbf{f}(\cdot)$ stands for the right-hand sides of (9-11, 17-20, 23) and $\mathbf{h}(\cdot)$ is a vector of the output functions. The output functions are linear, thus we can write

$$\mathbf{z} = \mathbf{h}(\mathbf{x}) = \mathbf{H}\mathbf{x}, \tag{27}$$

where

$$\mathbf{H} = \begin{bmatrix} 1 & 0 & 0 & 0 & 0 & 0 & 0 & 0 \\ 0 & 0 & 0 & 0 & 1 & 0 & 0 & 0 \\ 0 & 0 & 0 & 0 & 0 & 0 & 1 & 0 \\ 0 & 0 & 0 & 0 & 0 & 0 & 0 & 1 \end{bmatrix}. \tag{28}$$

E. Cabin and HVAC reference model in Dymola

A reference model of the FEV cabin and HVAC system was set up in Dymola using the `ThermalSystems` library, which was extended to suit the requirements (air quality modelling, additional temperature measurements). The Dymola model is significantly more complicated compared to the differential equations in previous subsections. The model was exported into a Functional Mockup Unit (FMU), which was then imported into the MATLAB Simulink environment using the FMUtoolbox [34]. The FMU represents a black box model of the cabin and HVAC system and is used as a substitution of a real FEV cabin and HVAC system for algorithms' verification.

An overview of the Dymola model is in Fig. 5, where the connectors were intentionally omitted to increase the clarity of the figure.

F. Simplified dynamic model verification

The simplified cabin and HVAC thermal models (subsections II-A and II-B) were compared to the Dymola reference model (subsection II-E). The results of the simulations are presented in Fig. 6 and Fig. 7.

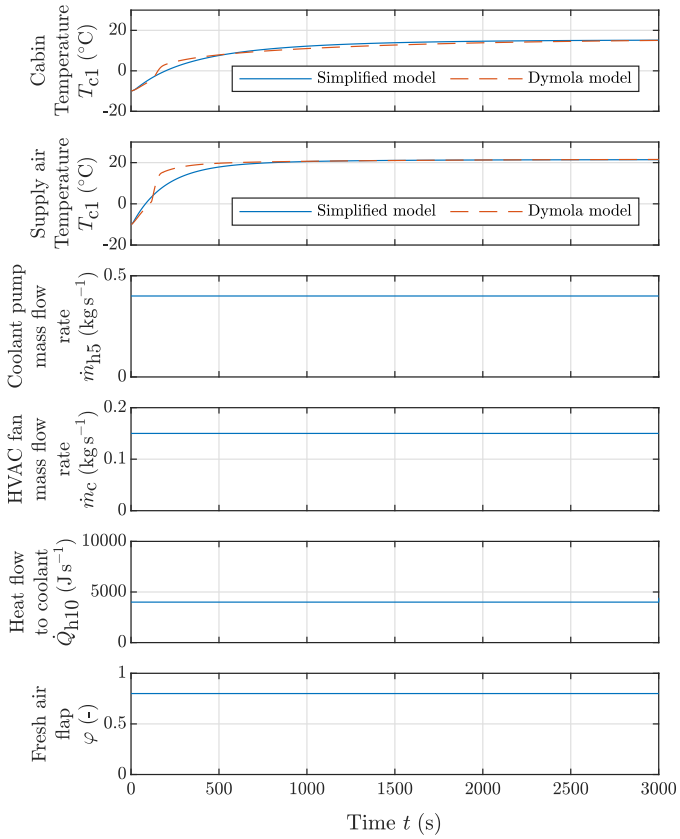

Fig. 6: Simplified HVAC and cabin model verification against Dymola reference model during cabin heat build-up

In Fig. 6 a cabin heat build-up is shown. This simulation result is included to show the conformity of the simplified model and Dymola model on the long term horizon. The control inputs were kept constant during the whole simulation. We can see that there is a small inaccuracy of both the cabin air temperature and supply air temperature at the time of 180 s, but the overall conformity of the models is satisfactory.

In Fig. 7 there is a simulation showing actuators changes and the reaction of both the dynamic models. There are almost no significant deviations of the simplified model and the reference Dymola model.

Thus we can conclude that the simplified model shows very good conformity to the reference Dymola model and it can be used for NMPC algorithm design.

III. NMPC PROBLEM FORMULATION

At each time step of the NMPC algorithm, an optimal control problem (OCP) needs to be solved [35]

$$\begin{aligned}\min J_N(\mathbf{x_0}, \mathbf{u}(\cdot)) = &\sum_{k=0}^{N-1} \|\mathbf{l}(\mathbf{x}_k, \mathbf{u}_k) - \mathbf{r}_k\|^2_{\mathbf{Q}} \\ &+ \|\mathbf{l}_N(\mathbf{x}_N) - \mathbf{r}_N\|^2_{\mathbf{Q}_N}, \end{aligned} \tag{29}$$

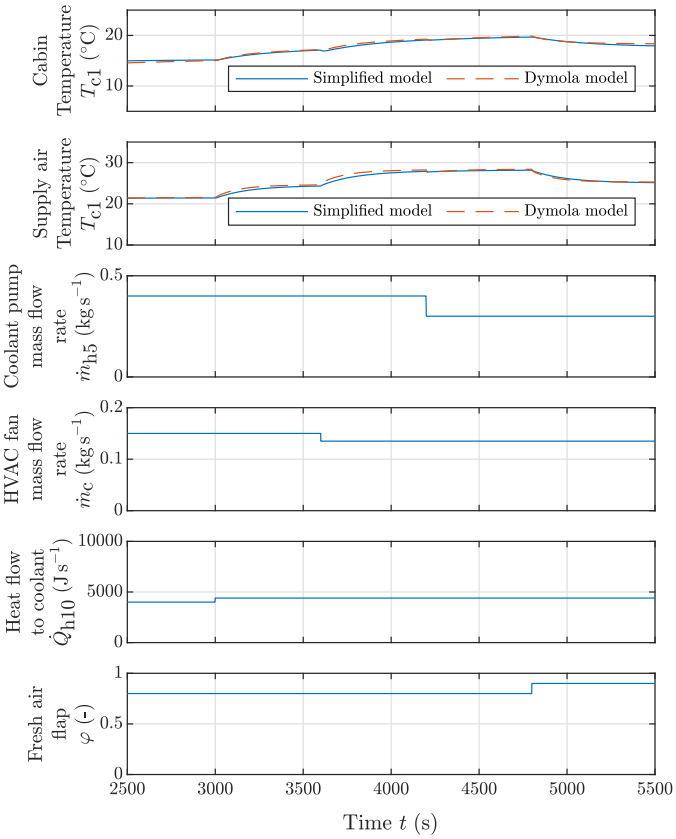

Fig. 7: Simplified HVAC and cabin model verification against Dymola reference model for actuators' changes

subject to

$$\mathbf{x}_0 = \hat{\mathbf{x}}_0, \tag{30}$$
$$\mathbf{x}_{k+1} = \mathbf{f}(\mathbf{x}_k, \mathbf{u}_k), \tag{31}$$
$$\mathbf{x}_k^{\text{lo}} \leq \mathbf{x}_k \leq \mathbf{x}_k^{\text{up}}, \tag{32}$$
$$\mathbf{u}_k^{\text{lo}} \leq \mathbf{u}_k \leq \mathbf{u}_k^{\text{up}}, \tag{33}$$

where $\mathbf{l}(\cdot)$ and $\mathbf{l}_N(\cdot)$ are vectors of penalized variables, $\mathbf{r}_k$ and $\mathbf{r}_N$ stand for time-varying and final references, $\mathbf{Q}$ and $\mathbf{Q}_N$ are weighting matrices. Then $\mathbf{x}$ denotes the discrete states, $\mathbf{u}$ the control input. Both the states and control inputs can be constrained by (32) and (33).

To allow constraints on control changes and their penalization, the model was slightly modified. The controls $\mathbf{u} = \begin{bmatrix}\dot{m}_{h5} & \dot{m}_c & \dot{Q}_{h10} & \varphi\end{bmatrix}^\mathsf{T}$ are now considered as additional states and we use a new controls vector $\Delta\mathbf{u} = \begin{bmatrix}\Delta\dot{m}_{h5} & \Delta\dot{m}_c & \Delta\dot{Q}_{h10} & \Delta\varphi\end{bmatrix}^\mathsf{T}$ and the additional set of differential equations

$$\frac{\mathrm{d}}{\mathrm{d}t}\begin{bmatrix}\dot{m}_{h5}\\ \dot{m}_c\\ \dot{Q}_{h10}\\ \varphi\end{bmatrix} = \begin{bmatrix}\Delta\dot{m}_{h5}\\ \Delta\dot{m}_c\\ \Delta\dot{Q}_{h10}\\ \Delta\varphi\end{bmatrix}. \tag{34}$$

This approach allows us to define constraints on control input changes, which is important when considering real actuators such as the air flap, coolant pump, etc., which have a limited control input change rate. Moreover, it is possible to introduce penalization of these changes, as fast changes are not convenient (especially for mechanical actuators).

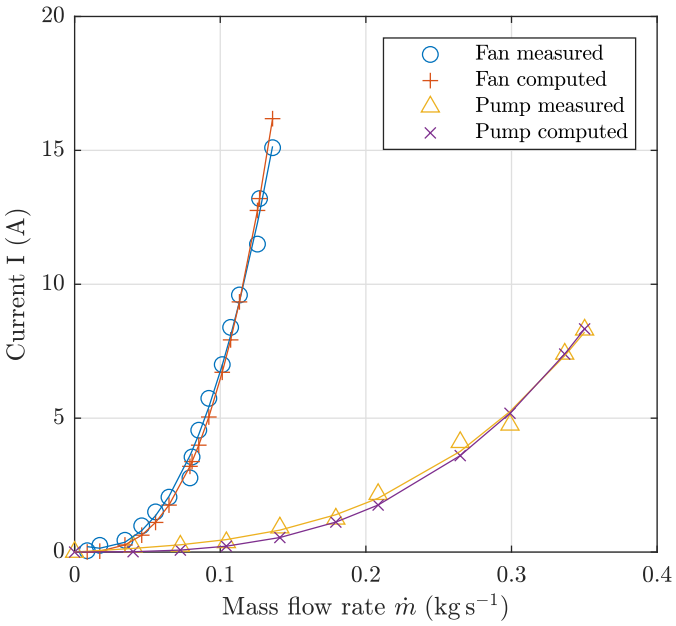

Fig. 8: HVAC fan and coolant pump current measurements and approximations

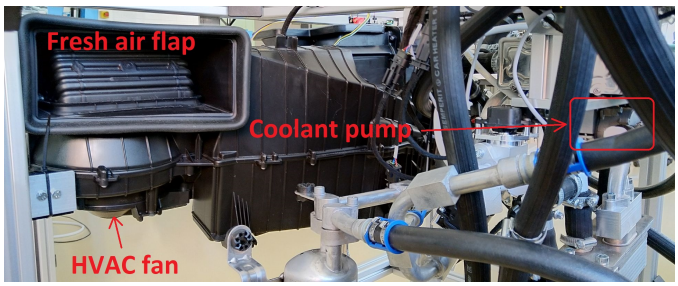

Fig. 9: FEV HVAC test bench (used for actuators' electric current dependency calibration and power consumption assessment, not for experimental verification)

The previously described change of control variables also ensures a zero steady-state error (offset free tracking), as shown, for example, in [36].

The model of the HVAC fan and coolant pump was calibrated on a test bench (Fig. 9) with real components by measurement of their characteristics (with focus on power consumption). The resulting data are shown in Fig. 8 (labelled as "measured").

Then a formula describing the dependency of electric current on mass flow rate was found for each of these actuators, to allow their comparison (under a constant input voltage $U = 12\,\text{V}$). Both the fan and pump employ a fan load characteristic, which means that motor torque is dependent on the squared angular speed, and the input power (and thus current) depends on the third power of angular speed. The volumetric flow rate and mass flow rate are approximately linearly dependent on the fan/pump motor angular speed. The

HVAC fan electric current can be written as

$$I_{\text{fan}} = a_{\text{fan}}(\dot{m}_{\text{fan}})^3, \tag{35}$$

where I_{fan} is the electric current of the HVAC fan, a_{fan} is a constant characterizing the fan and HVAC air distribution box (in our case, $a_{\text{fan}} = 6443$). Then $\dot{m}_{\text{fan}}$ is the air mass flow rate through the fan.

The coolant pump electric current can be described by

$$I_{\text{pump}} = a_{\text{pump}}(\dot{m}_{\text{pump}})^3, \tag{36}$$

where I_{pump} is the electric current of the coolant pump, a_{pump} is a pump and pipes constant (in our case, $a_{\text{pump}} = 194$), and $\dot{m}_{\text{pump}}$ is the coolant mass flow rate caused by the pump.

The specific values of the fan and pump constants (a_{fan} and a_{pump}) were acquired by fitting the general formulae to measured electric current. The comparison of measured values and results from (35) and (36) are in Fig. 8, and the correspondence is satisfactory.

From (35) and (36) it is evident that the penalization of the HVAC fan should be approximately thirty times higher compared to the coolant pump to ensure comparability of power consumption.

To accomplish the basic goal of energy efficient control, the overall power consumption needs to be minimized. This can be computed as

$$P_{\text{el}} = P_{\text{fan}} + P_{\text{pump}} + P_{\text{heat}}, \tag{37}$$

where P_{el} is overall electric power consumption, P_{fan} and P_{pump} are electric power consumptions of HVAC the fan and pump respectively, and P_{heat} stands for electric power consumption of the heat source utilized to provide heat flow $\dot{Q}_{\text{h10}}$. After minor modifications and substitutions, we can write

$$P_{\text{el}} = U[a_{\text{fan}}(\dot{m}_{\text{c}})^3 + a_{\text{pump}}(\dot{m}_{\text{h5}})^3] + \frac{\dot{Q}_{\text{h10}}}{COP}, \tag{38}$$

where $U = 12\,\text{V}$ is battery voltage and COP stands for coefficient of performance

$$COP = \frac{|Q|}{W}, \tag{39}$$

where Q is the heat supplied to the coolant and W is the work required for that. If we consider purely electric heating, $COP = 1$, for heat pump systems, we expect $COP \in (1.5, 3)$.

The contribution of actuators to overall electric power consumption is illustrated in Fig. 10 for maximal values of actuators speed (causing maximal power consumption). In this example heat pump system is considered, if the PTC heater was a heat source, its percentage would be much higher.

The resulting vectors of penalized variables are

$$\mathbf{l}(\mathbf{x}_k, \mathbf{u}_k) = \begin{bmatrix}\mathbf{x}_{\text{l}}^\intercal & \mathbf{u}_{\text{l}}^\intercal & \Delta\mathbf{u}_{\text{l}}^\intercal\end{bmatrix}^\intercal, \tag{40}$$

$$\mathbf{l}_N(\mathbf{x}_k) = \begin{bmatrix}\mathbf{x}_{\text{l}}^\intercal & \mathbf{u}_{\text{l}}^\intercal\end{bmatrix}^\intercal, \tag{41}$$

where penalized state vector is

$$\mathbf{x}_{\text{l}} = \mathbf{R}_x \mathbf{x}_k, \tag{42}$$

penalized controls vector

$$\mathbf{u}_{\text{l}} = \mathbf{R}_u \mathbf{u}_k, \tag{43}$$

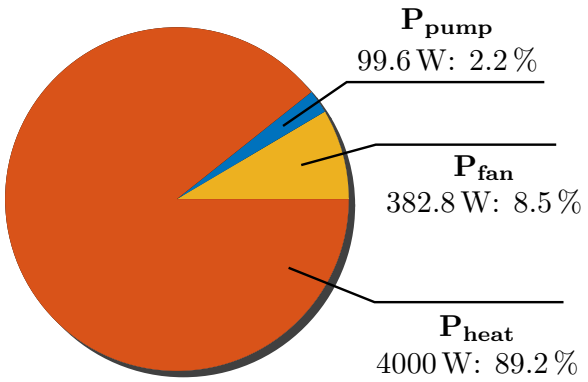

Fig. 10: Maximal power consumption of heating actuators, for a heat pump with $COP = 2$ and maximal thermal power $\dot{Q}_{\text{h10}} = 8000\,\text{W}$

and penalized controls change vector

$$\Delta\mathbf{u}_{\text{l}} = \mathbf{R}_{\Delta u}\Delta\mathbf{u}_k, \tag{44}$$

with $\mathbf{R}$ being the helper scaling matrices.

The weighting matrices $\mathbf{Q}$ and $\mathbf{Q}_N$ were initially set up with respect to (38), and then fine-tuned considering the user comfort point of view - the fan speed penalization was increased. Thus, the weighting matrices were slightly changed to fulfill all the requirements defined in section I. As a result, the power consumption would probably not be the optimal, but we can reach a satisfactory suboptimal trajectory of the system with accomplishment of the user requirements.

The following set of state constraints was introduced

$$0 \le T_{\text{h4}} \le 273.15 + 90 \quad (\text{K}), \tag{45}$$

$$0 \le T_{\text{h1}} \le 273.15 + 60 \quad (\text{K}), \tag{46}$$

which represent the maximum allowed temperatures of coolant and supplied air respectively. The control constraints

$$0.04 \le \dot{m}_{\text{h5}} \le 0.42 \quad (\text{kg s}^{-1}), \tag{47}$$

$$0.03 \le \dot{m}_{\text{c}} \le 0.17 \quad (\text{kg s}^{-1}), \tag{48}$$

$$0 \le \dot{Q}_{\text{h10}} \le 8000 \quad (\text{J s}^{-1}), \tag{49}$$

$$0 \le \varphi \le 1 \quad (-), \tag{50}$$

respect the real possibilities of the considered system. The coolant and air mass flow rates were measured on our test bench (Fig. 9), the heat flow rate is a guessed value for a heat pump system and can be adjusted based on the heating device (heat pump, PTC, etc.). The fresh air ratio range is derived from its definition.

Then we also introduce constraints on the control changes

$$-0.05 \le \Delta\dot{m}_{\text{c}} \le 0.05 \quad (\text{kg s}^{-2}), \tag{51}$$

$$-0.05 \le \Delta\dot{m}_{\text{h5}} \le 0.05, \quad (\text{kg s}^{-2}) \tag{52}$$

$$-400 \le \Delta\dot{Q}_{\text{h10}} \le 400 \quad (\text{J s}^{-2}), \tag{53}$$

$$-0.1 \le \Delta\varphi \le 0.1 \quad (\text{s}^{-1}), \tag{54}$$

which also respect the real system capabilities, such as maximum possible fan and pump acceleration, fresh flap speed, etc.

We introduce the reference vector

$$\mathbf{r} = \begin{bmatrix}\mathbf{r}_\mathbf{x}^\intercal & \mathbf{r}_\mathbf{u}^\intercal & \mathbf{r}_{\mathbf{\Delta u}}^\intercal\end{bmatrix}^\intercal \tag{55}$$

with state references $\mathbf{r_x}$, controls references $\mathbf{r_u}$ and controls change references $\mathbf{r_{\Delta u}}$

$$\mathbf{r_x} = \begin{bmatrix}r_{T_{\mathrm{c1}}} & 0 & 0 & 0 & 0 & 0 & r_{T_{\mathrm{h4}}} & 0 & r_\kappa\end{bmatrix}^\intercal, \tag{56}$$

$$\mathbf{r_u} = \begin{bmatrix}0 & 0 & 0 & 0\end{bmatrix}^\intercal, \tag{57}$$

$$\mathbf{r_{\Delta u}} = \begin{bmatrix}0 & 0 & 0 & 0\end{bmatrix}^\intercal, \tag{58}$$

where $r_{T_{\mathrm{c1}}}$ is the cabin temperature reference, r_κ is the cabin air quality reference and, $r_{T_{\mathrm{h4}}}$ is the coolant temperature reference.

The sampling rate was chosen as $T_\mathrm{s} = 0.5\,\mathrm{s}$ to cover the fastest dynamics in the controlled system. In combination with a prediction horizon $N = 20$, we get a prediction time of $10\,\mathrm{s}$. The `ACADO toolkit` [37] (including MATLAB interface) was used for implementation in MATLAB/Simulink, and also for C/C++ code generation. A multiple shooting technique [38] was used for discretization of the continuous-time model. A quadratic programming solver, `qpOASES` [39], employing an active-set method [40], was used to solve the optimization problem.

IV. Extended Kalman Filter

The Extended Kalman Filter (EKF) from [41] was used to allow current system states estimation, as they are needed for NMPC computations.

The part of the state variables from (26) can be directly measured (cabin air temperature T_{c1}, supply air temperature T_{h1}, heated coolant temperature T_{h4}, and cabin air quality κ), the rest of the temperatures (four of them) needs to be estimated by EKF.

A discrete-time system model

$$\mathbf{x}_k = \mathbf{f}(\mathbf{x}_{k-1}, \mathbf{u}_{k-1}) + \mathbf{w}_k, \tag{59}$$

$$\mathbf{z}_k = \mathbf{h}(\mathbf{x}_k) + \mathbf{v}_k, \tag{60}$$

is needed for both the phases (prediction and update) of the EKF. The model described above was discretized using the Euler method in order to get a discrete-time model of the vehicle cabin and HVAC system.

Then we use the following equations for the prediction phase of the EKF

$$\hat{\mathbf{x}}_k^- = \mathbf{f}(\mathbf{x}_{k-1}, \mathbf{u}_k, 0), \tag{61}$$

$$\mathbf{P}_k^- = \mathbf{F}_{k-1}\mathbf{P}_{k-1}\mathbf{F}_{k-1}^\intercal + \mathbf{Q}_{k-1}, \tag{62}$$

and the second set of equations for the update phase

$$\mathbf{K}_k = \mathbf{P}_k^-\mathbf{H}^\intercal(\mathbf{H}\mathbf{P}_k^-\mathbf{H}^\intercal + \mathbf{R})^{-1}, \tag{63}$$

$$\hat{\mathbf{x}}_k = \hat{\mathbf{x}}_k^- + \mathbf{K}_k(\mathbf{z}_k - \mathbf{H}\hat{\mathbf{x}}_k^-), \tag{64}$$

$$\mathbf{P}_k = (\mathbf{I} - \mathbf{K}_k\mathbf{H})\mathbf{P}_k^-, \tag{65}$$

where $\hat{\mathbf{x}}_k^-$ and $\hat{\mathbf{x}}_k$ are the a priori and a posteriori state estimates respectively, $\mathbf{P}_k^-$ and $\mathbf{P}_k$ are the a priori and a posteriori estimate error covariance matrices, $\mathbf{F}_{k-1}$ is the Jacobian of function $\mathbf{f}(\cdot)$, $\mathbf{Q}_{k-1}$ stands for the process noise covariance matrix, $\mathbf{K}_k$ is the Kalman gain, $\mathbf{R}$ is the measurement error covariance matrix. As the function $\mathbf{h}(\cdot)$ is linear, the last term in (64) was reduced to the product of matrix $\mathbf{H}$ and the a priori state estimate $\hat{\mathbf{x}}_k^-$ (compared with the standard $\mathbf{h}(\hat{\mathbf{x}}_k^-, 0)$ term).

The ambient temperature ($T_{\mathrm{h5}} = T_{\mathrm{c5}}$) can be considered as a measured disturbance, since this variable behaves as an input to our models (can change in time, it is not a constant, but we can not influence its value). Thus, we incorporate it as a measured state with a zero time derivative and its value is obtained by the EKF. The following equation was added to the set of the differential equations

$$\frac{\mathrm{d}T_{\mathrm{c5}}}{\mathrm{d}t} = 0, \tag{66}$$

where T_{c5} is the ambient temperature.

V. Simulations

The simulations described within this section were realized in the MATLAB/Simulink environment.

The cabin and HVAC model was exported from Dymola into the Functional Mockup Unit (FMU) exchange format and then imported into Simulink using the `FMUtoolbox` [34], a self-developed FMU importing tool for Matlab/Simulink.

A. Model in the Loop

A Model in the Loop (MIL) simulation was the starting point during the NMPC algorithms tuning. As a first step, the NMPC algorithms were tested in a pure MATLAB environment (m-file script). This step was important for tuning the very base functionality - constraints, first guess of penalization matrices, etc.

The NMPC controller was connected to the same plant (cabin and HVAC) model that was used for the controller assembly. Thus the state observer was not necessary and the changes of the model and other settings are quite simple.

The main advantage of the MIL simulation is the speed of deployment, as C++ code generated based on an m-file script is automatically built into the mex-file and then simulated under the MATLAB environment with the possibility to easily plot the simulation results.

B. Software in the Loop

Software in the Loop (SIL) simulation was performed in the MATLAB Simulink environment with usage of the C S-function. The `ACADO Code Generation tool` was used to export the highly efficient C-code for NMPC implementation.

As a plant model, the Dymola model of the cabin and HVAC was used. The model needs the actuator values as inputs, but the controller provides only the changes of actuator values. The discrete integration of actuator values was added to the EKF algorithms.

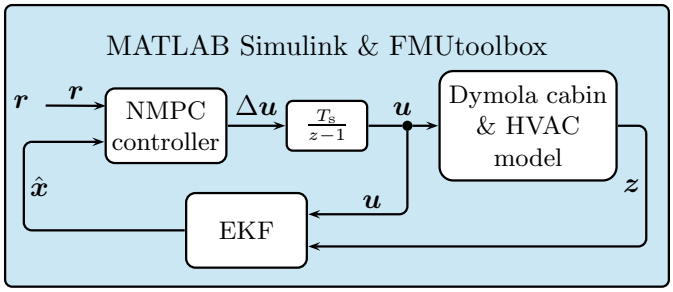

Fig. 11: SIL simulation diagram

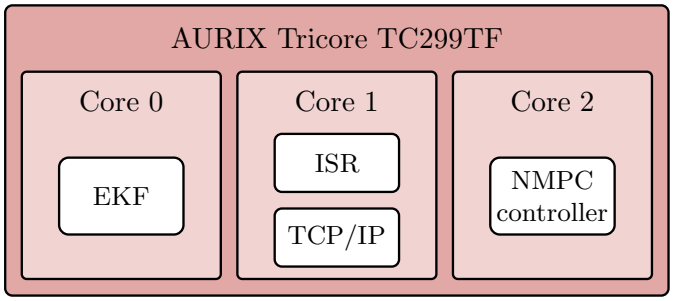

Fig. 12: AURIX Tricore tasks overview

C. Processor in the Loop

The NMPC algorithms were successfully implemented on an Infineon AURIX Tricore TC299TF microcontroller unit (MCU), placed on the AURIX Starter Kit TC299. The MCU contains three cores running at 300 MHz, 8 MB FLASH (4x2 MB) and 728 kB RAM.

The software tasks were divided between the MCU cores as shown in Fig. 12. Core 1 provides timing based on interrupts for the other cores (shown as an interrupt service routine (ISR) task), by setting the execution flags at a defined frequency. This core also ensures the TCP/IP communication with the MATLAB Simulink (illustrated in Fig. 13). Core 0 is responsible for EKF execution and the NMPC algorithms are running within Core 2.

In Fig. 13, there is a diagram of the Processor in the Loop (PIL) simulation. The references ($\mathbf{r}$) and measured outputs ($\mathbf{z}$) from the Dymola model (running under MATLAB/Simulink) are sent to the MCU via TCP/IP communication, and the controls ($\mathbf{u}$) are sent from the MCU to the MATLAB Simulink and applied to the Dymola model. As mentioned before (SIL simulation), the controls from the NMPC controller have to be discretely integrated before applying them to the Dymola model.

In Fig. 14, there is a photo of the AURIX Starter Kit TC299 that was used as the target of the control algorithms described within this paper. The board is connected via TCP/IP (see Fig. 13) with a PC, on which the MATLAB/Simulink environment and Dymola model are running. Moreover, there are debug and power lines.

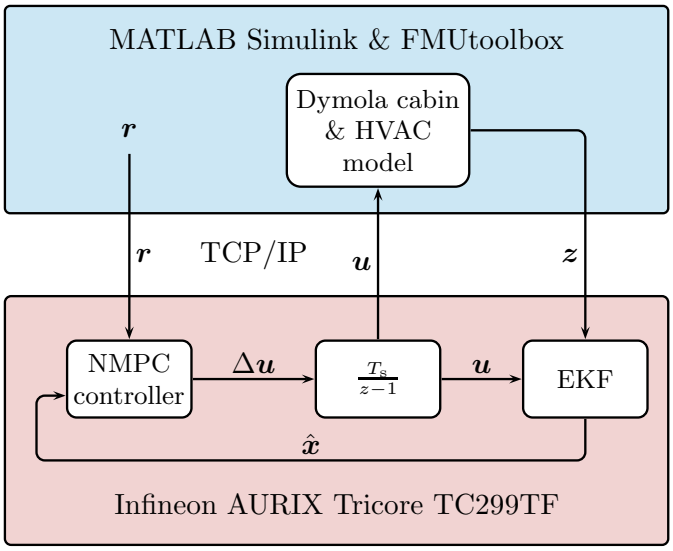

Fig. 13: PIL simulation diagram

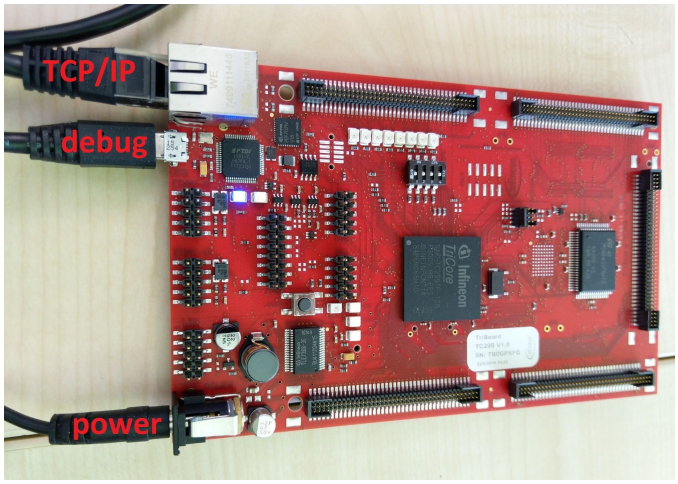

Fig. 14: PIL simulation target - Infineon AURIX TC299TF on the AURIX Starter Kit TC299

D. FEV cabin heat build-up

In Fig. 15 there are results of a simulation of FEV cabin heat build-up. The simulation conditions were defined as an average winter day with ambient temperature of $-10\,°\mathrm{C}$, and this temperature was also used as the initial temperature of the whole vehicle cabin and other equipment. Two passengers are considered, and no solar flow is present during the simulation.

The cabin temperature reference ($r_{T_{\mathrm{cl}}} = 20\,°\mathrm{C}$) was achieved after approx. 200 s, which is quite an impressive value. This fast heat build-up is possible thanks to the fully closed fresh air flap, which has the drawback of slightly degraded air quality (above 1000 ppm; limited for a short time). The air quality is improved immediately after the cabin temperature settles and then it is kept approximately at the reference value of 900 ppm.

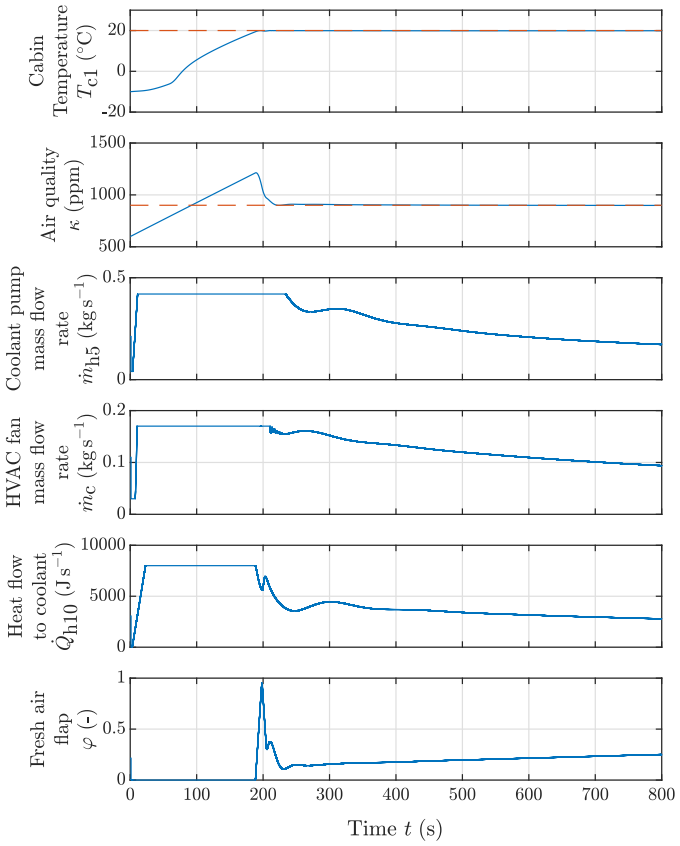

Fig. 15: NMPC PIL simulation of cabin heat build-up with ambient temperature $T_{c5} = -10\,°C$, two passengers inside the cabin and no solar heat flow

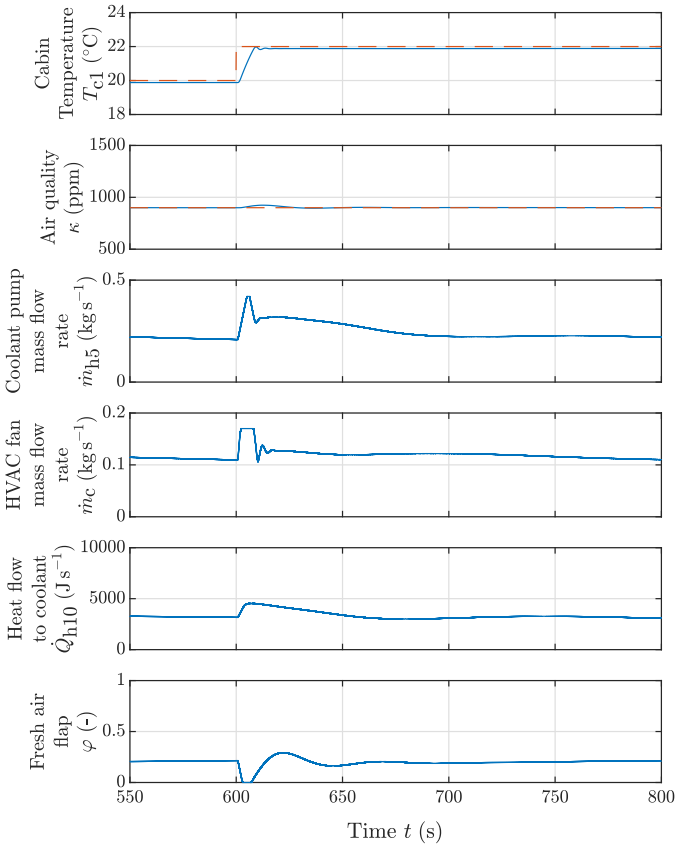

Fig. 16: PIL simulation of cabin temperature reference step

E. Temperature reference change

Fig. 16 presents the temperature reference change of $2\,°C$ and the reaction of the NMPC algorithms to this change. The reference change occurred at the time of $600\,s$, and the new reference value of the cabin air temperature was reached after a very short time, which is possible by coordination of all the actuators. Both the coolant pump and HVAC fan were speeded up, heat flow to the coolant was increased by $1200\,W$ for a short time, and the fresh air flap was closed during the temperature increase.

The benefits of NMPC are evident from this case, as multivariable control helps to reduce the time needed for change of the cabin air temperature. Also, there is no overshoot and all of the variables are natively kept within the defined constraints.

F. Disturbance rejection

Two most common disturbances were selected for presentation. The first one is shown in Fig. 17, and was caused by increasing the number of passengers in the vehicle. Both the cabin air temperature and quality are affected by this change, and it can be seen that the temperature is kept approx. at the defined reference, the air quality got slightly worse, and there remains some steady state error. This is caused by a conservative penalization value of the air quality, as it doesn't have to strictly track the reference, but it needs to be kept within a reasonable range (e.g. $800\,ppm$ to $1200\,ppm$). Thus, the steady state error is the trade-off between the air quality and the power consumption needed for cabin heating. The fresh air flap position was moved from approx. $20\,\%$ to $50\,\%$ as an appropriate response to this disturbance.

The second disturbance is represented by ambient temperature change, which affects both the thermal losses through the cabin walls and the inlet fresh air temperature. In Fig. 18, there are results of the simulation with a step change of ambient temperature at the time of $600\,s$ from $-10\,°C$ to $0\,°C$. Both the cabin temperature and air quality track the references, and only the decrease of the heat flow $\dot{Q}_{h10}$ is perceptible.

VI. Conclusion

This article introduced Non-linear Model Predictive Control for Fully Electric Vehicle cabin temperature and air quality control. The final solution is suboptimal from an electric energy consumption perspective, as passenger comfort was also taken into account during algorithm tuning.

The novel contribution of the paper is the idea of an integrated approach to cabin comfort control (temperature and air quality), which can bring significant energy savings. Also, the air quality model, which was developed by us and used for NMPC algorithms design, is a significant benefit of the paper. The particular energy saving will depend on many different conditions (ambient air quality, vehicle occupancy, ambient

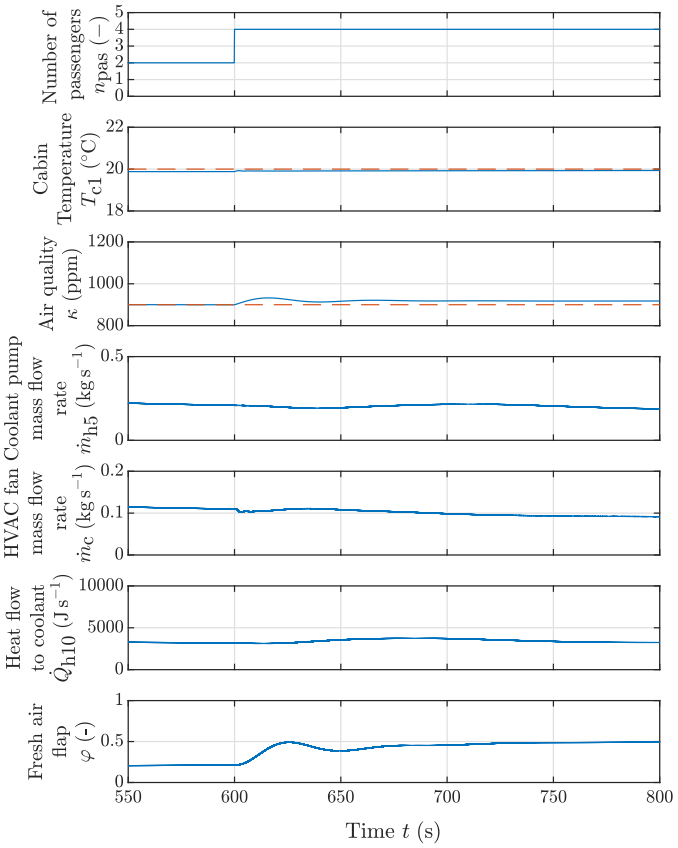

Fig. 17: PIL simulation of disturbance rejection - increase in the number of cabin passengers

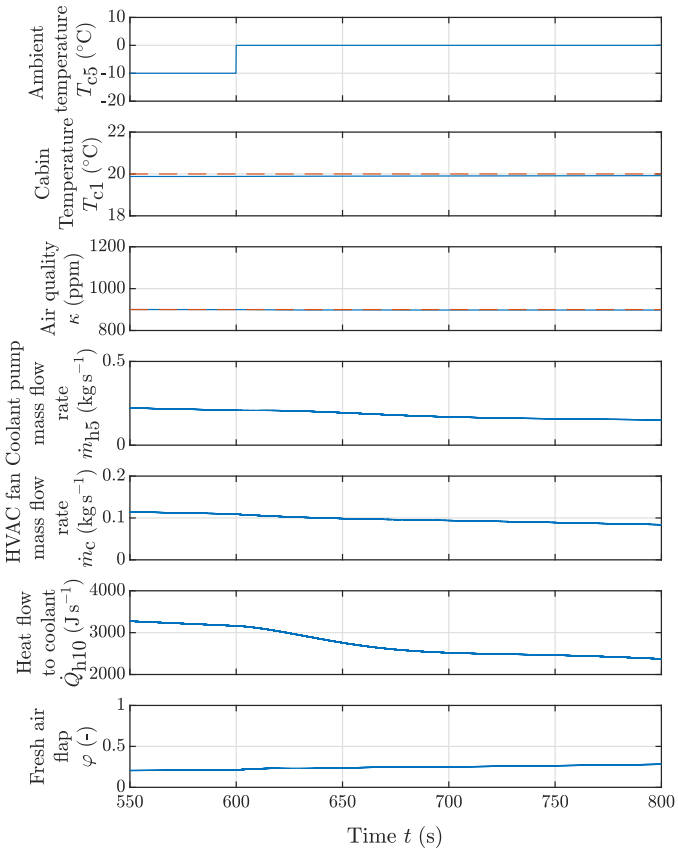

Fig. 18: PIL simulation of disturbance rejection - ambient temperature change

temperature, etc.) and there is no common methodology for HVAC consumption evaluation.

For a brief overview of our approach performance from an energy consumption perspective, we defined a test case consisting of an hour drive under cold conditions to demonstrate the possibilities of energy savings. This test case was simulated with different cabin air quality reference and the results are shown in Fig. 19. In accordance with our expectations, air quality reference has a strong influence on HVAC overall power consumption. If we consider cabin air quality reference of 900 ppm, an energy saving of 41.3 % can be achieved for the defined test case. It should be reminded that this particular number is only valid for a defined situation and the real savings will be different due to several reasons. Firstly, the power consumption is strongly dependent on ambient and initial conditions. Secondly, a fully open fresh flap is taken as the baseline (which might not fit all the EVs). Thirdly, energy savings significantly depend on vehicle occupancy. Even though the numbers could be different, our approach would save as much energy as possible under any operating and ambient conditions (considering the energy losses by cabin ventilation).

The control algorithms were implemented into an automotive qualified microcontroller, the Infineon AURIX Tricore TC299TF, and the performance of the algorithms was demonstrated employing Processor in the Loop simulations.

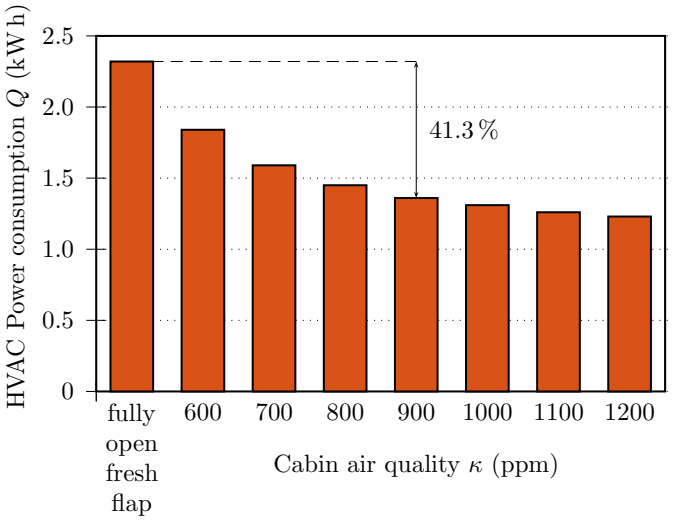

Fig. 19: Possible energy savings using NMPC strategy. Simulated for single typical configuration: 3600 s vehicle drive (including cabin heat build-up), initial cabin temperature of −10 °C, cabin temperature reference of 20 °C, ambient temperature of −10 °C, 2 passengers in the cabin, ambient air quality of 400 ppm, initial cabin air quality of 600 ppm.

This control approach can substantially help to avoid electric vehicle range decrease under cold conditions by minimiz-

ing the amount of exhausted air and thus minimizing the heat losses through cabin ventilation. In combination with other approaches (cabin insulation, heat pump systems, waste heat recovery, thermal energy storage), it could reduce the disadvantage of electric vehicles during the winter season. Despite that the approach was aimed at Fully Electric Vehicles equipped with a heat pump system, it could be (with minor changes) used in any other vehicles (hybrid, fuel cell, etc.; with a PTC heater or any other heat source), and even in other transportation modes (trains, buses, etc.).

At the moment, the proposed approach was verified only in simulations (MIL, SIL, and PIL) as it was not so far possible to modify our test bench to allow experimental verification (it would require a cabin with passengers, which is difficult to install at our facility). The final application into a Mercedes-Benz B-Class Electric Drive (W 242) vehicle is planned and it would require some changes to the fresh air flap shape, as the current shape does not allow precise control of the fresh air ratio. Also, it would be necessary to install an air quality sensor into the vehicle cabin. We plan to push this control approach to the next level by either modifying our test bench or implementing it into a real vehicle to allow experimental verification of the algorithms.

Of course, there are possible improvements of the control strategy. For example, if the vehicle also contained an outdoor air quality sensor, then it would enable advanced indoor air quality control (the vehicle cabin could be ventilated intensively in fresh air areas). Then, there is the possibility of incorporating cabin humidity modelling and control into the NMPC algorithms. That would allow the possibility of automatic fogging detection and dehumidification control, which would improve the user experience.

The presented approach is suitable for vehicle standstill conditions, however, during the vehicle movement, the HVAC system performance might be influenced by vehicle speed in terms of HVAC air mass flow rate, higher cabin cooling due to forced convection, and different heat pump coefficient of performance (COP). For a final implementation, the mitigation of these influences would require to measure disturbance air mass flow rate under different vehicle speeds (for a particular vehicle) and integration of this dependency into the HVAC model. The higher heat flow rate to the ambient caused by forced convection could be assumed as a process disturbance (which the NMPC can deal with). It would be also possible to measure the effect of forced convection on thermal losses and incorporate it into the cabin model. If the vehicle was equipped with a heat pump system, it would be useful to dynamically adjust weighting matrices according to current operating conditions (i.e. COP), which should help the NMPC algorithms to operate efficiently independently on the vehicle speed.

The difference between system time constants (units up to hundreds of seconds) can in the future development lead to multi-level NMPC algorithms with different sampling periods (short for heat exchangers, larger for vehicle cabin). As a final possible improvement, we see the variant coolant temperature reference $r_{T_{\mathrm{h4}}}$. Currently, it has a constant value ($r_{T_{\mathrm{h4}}} = 50\,^{\circ}\mathrm{C}$), but it has very low penalization, thus the temperature T_{h4} usually exceeds its reference (especially during cabin heat build-up). We propose to use equitherm regulation, which would set up the coolant temperature reference based on ambient temperature and a preconfigured equitherm curve. This improvement could bring some energy savings due to lower heat losses, but it will require detailed measurements for equitherm curve assembly.

ACKNOWLEDGEMENT

This research was carried out under the project H2020 653514 OSEM-EV - Optimised and Systematic Energy Management in Electric Vehicles and under the project LQ1601 CEITEC 2020.

The work was supported by the infrastructure of RICAIP that has received funding from the European Union's Horizon 2020 research and innovation program under grant agreement No 857306 and from the Ministry of Education, Youth and Sports under OP RDE grant agreement No CZ.02.1.01/0.0/0.0/17_043/0010085.

REFERENCES

[1] W. Adaileh and A. Alahmer, "Recovery of Exhaust Waste Heat for ICE Using the Beta Type Stirling Engine," *Journal of Energy*, vol. 2015, p. Article ID 495418, 2015.

[2] K. T. Chau and C. C. Chan, "Emerging Energy-Efficient Technologies for Hybrid Electric Vehicles," *Proceedings of the IEEE*, vol. 95, no. 4, pp. 821–835, Apr. 2007.

[3] J. Martins, F. P. Brito, D. Pedrosa, V. Monteiro, and L. João, "Real-Life Comparison Between Diesel and Electric Car Energy Consumption," in *Grid Electrified Vehicles: Performance, Design and Environmental Impacts*. Nova Science Publishers, 2013, no. December 2015, pp. 209–232.

[4] M. Åhman, "Primary energy efficiency of alternative powertrains in vehicles," *Energy*, vol. 26, no. 11, pp. 973–989, Nov. 2001.

[5] Z. Zhang, J. Wang, X. Feng, L. Chang, Y. Chen, and X. Wang, "The solutions to electric vehicle air conditioning systems: A review," *Renewable and Sustainable Energy Reviews*, vol. 91, pp. 443–463, Aug. 2018.

[6] C. Goh, L. Kamarudin, S. Shukri, N. Abdullah, and A. Zakaria, "Monitoring of carbon dioxide (CO2) accumulation in vehicle cabin," in *2016 3rd International Conference on Electronic Design (ICED)*. IEEE, Aug. 2016, pp. 427–432.

[7] S. Schaut and O. Sawodny, "Thermal Management for the Cabin of a Battery Electric Vehicle Considering Passengers' Comfort," *IEEE Transactions on Control Systems Technology*, vol. 28, no. 4, pp. 1476–1492, Jul. 2020.

[8] B. C. Ng, I. Z. M. Darus, H. Jamaluddin, and H. M. Kamar, "Application of adaptive neural predictive control for an automotive air conditioning system," *Applied Thermal Engineering*, vol. 73, no. 1, pp. 1244–1254, Dec. 2014.

[9] M. R. Amini, H. Wang, X. Gong, D. Liao-McPherson, I. Kolmanovsky, and J. Sun, "Cabin and Battery Thermal Management of Connected and Automated HEVs for Improved Energy Efficiency Using Hierarchical Model Predictive Control," *IEEE Transactions on Control Systems Technology*, 2019.

[10] H. He, M. Yan, C. Sun, J. Peng, M. Li, and H. Jia, "Predictive air-conditioner control for electric buses with passenger amount variation forecast," *Applied Energy*, vol. 227, pp. 249–261, Oct. 2018.

[11] H. Wang, I. Kolmanovsky, M. R. Amini, and J. Sun, "Model Predictive Climate Control of Connected and Automated Vehicles for Improved Energy Efficiency," in *Proceedings of the American Control Conference*, vol. 2018-June. Institute of Electrical and Electronics Engineers Inc., Aug. 2018, pp. 828–833.

[12] J. Lopez Sanz, C. Ocampo-Martinez, J. Alvarez-Florez, M. Moreno Eguilaz, R. Ruiz-Mansilla, J. Kalmus, M. Graber, and G. Lux, "Non-linear Model Predictive Control for Thermal Management in Plug-in Hybrid Electric Vehicles," *IEEE Transactions on Vehicular Technology*, pp. 1–1, 2016.

[13] J. Lopez-Sanz, C. Ocampo-Martinez, J. Alvarez-Florez, M. Moreno-Eguilaz, R. Ruiz-Mansilla, J. Kalmus, M. Graeber, and G. Lux, "Thermal Management in Plug-In Hybrid Electric Vehicles: A Real-Time Nonlinear Model Predictive Control Implementation," *IEEE Transactions on Vehicular Technology*, vol. 66, no. 9, pp. 7751–7760, Sep. 2017.
[14] S. S. Butt, R. Prabel, and H. Aschemann, "Model-predictive on-off control of a combustion-heating-system for vehicles," in *2013 European Control Conference (ECC)*. IEEE, Jul. 2013, pp. 1988–1993.
[15] T. Fischer, T. Kraus, C. Kirches, and F. Gauterin, "Demonstration of a Nonlinear Model Predictive Control of a Thermal Management System for Electric Vehicles in Real-Time," in *2018 IEEE Conference on Control Technology and Applications (CCTA)*. IEEE, Aug. 2018, pp. 676–682.
[16] Y. Huang, A. Khajepour, F. Bagheri, and M. Bahrami, "Optimal energy-efficient predictive controllers in automotive air-conditioning/refrigeration systems," *Applied Energy*, vol. 184, pp. 605–618, Dec. 2016.
[17] K. Galatsis, W. Wlodarski, Yongxiang Li, and K. Kalantar-zadeh, "Ventilation control for improved cabin air quality and vehicle safety," in *IEEE VTS 53rd Vehicular Technology Conference, Spring 2001. Proceedings (Cat. No.01CH37202)*, vol. 4. IEEE, 2001, pp. 3018–3021.
[18] Jinjing Yang, Yu Chen, Yimin Liu, O. Makke, J. Yeung, O. Gusikhin, and P. MacNeille, "The effectiveness of cloud-based smart in-vehicle air quality management," in *2016 IEEE Advanced Information Management, Communicates, Electronic and Automation Control Conference (IMCEC)*. IEEE, Oct. 2016, pp. 325–329.
[19] D. Kolokotsa, A. Pouliezos, G. Stavrakakis, and C. Lazos, "Predictive control techniques for energy and indoor environmental quality management in buildings," *Building and Environment*, vol. 44, no. 9, pp. 1850–1863, Sep. 2009.
[20] J. Eckstein, C. Lüke, F. Brunstein, P. Friedel, and U. Köhler, "A Novel Approach Using Model Predictive Control to Enhance the Range of Electric Vehicles," *Procedia Technology*, vol. 26, pp. 177–184, Jan. 2016.
[21] S. Uebel, N. Murgovski, B. Bäker, and J. Sjöberg, "A Two-Level MPC for Energy Management Including Velocity Control of Hybrid Electric Vehicles," *IEEE Transactions on Vehicular Technology*, vol. 68, no. 6, pp. 5494–5505, Jun. 2019.
[22] M. Salazar, C. Balerna, P. Elbert, F. P. Grando, and C. H. Onder, "Real-time control algorithms for a hybrid electric race car using a two-level model predictive control scheme," *IEEE Transactions on Vehicular Technology*, vol. 66, no. 12, pp. 10 911–10 922, Dec. 2017.
[23] H. Wang, Y. Huang, A. Soltani, A. Khajepour, and D. Cao, "Cyber-Physical Predictive Energy Management for Through-the-Road Hybrid Vehicles," *IEEE Transactions on Vehicular Technology*, vol. 68, no. 4, pp. 3246–3256, Apr. 2019.
[24] D. M. Wu, Y. Li, C. Q. Du, H. T. Ding, Y. Li, X. B. Yang, and X. Y. Lu, "Fast velocity trajectory planning and control algorithm of intelligent 4WD electric vehicle for energy saving using time-based MPC," *IET Intelligent Transport Systems*, vol. 13, no. 1, pp. 153–159, Jan. 2019.
[25] C. Sun, X. Zhang, Q. Zhou, and Y. Tian, "A Model Predictive Controller with Switched Tracking Error for Autonomous Vehicle Path Tracking," *IEEE Access*, vol. 7, pp. 53 103–53 114, 2019.
[26] H. Wang, B. Liu, X. Ping, and Q. An, "Path Tracking Control for Autonomous Vehicles Based on an Improved MPC," *IEEE Access*, pp. 1–1, Oct. 2019.
[27] J. Felez, C. Garcia-Sanchez, and J. A. Lozano, "Control Design for an Articulated Truck with Autonomous Driving in an Electrified Highway," *IEEE Access*, vol. 6, pp. 60 171–60 186, 2018.
[28] B. Sakhdari and N. L. Azad, "Adaptive Tube-Based Nonlinear MPC for Economic Autonomous Cruise Control of Plug-In Hybrid Electric Vehicles," *IEEE Transactions on Vehicular Technology*, vol. 67, no. 12, pp. 11 390–11 401, Dec. 2018.
[29] D. Moser, R. Schmied, H. Waschl, and L. Del Re, "Flexible Spacing Adaptive Cruise Control Using Stochastic Model Predictive Control," *IEEE Transactions on Control Systems Technology*, vol. 26, no. 1, pp. 114–127, Jan. 2018.
[30] L. A. Incropera Frank P., Dewitt D.P., Bergman T. L., *Fundamentals of Heat and Mass Transfer*. John Wiley & Sons, 2011.
[31] P. A. Scheff, V. K. Paulius, S. W. Huang, and L. M. Conroy, "Indoor Air Quality in a Middle School, Part I: Use of CO2 as a Tracer for Effective Ventilation," *Applied Occupational and Environmental Hygiene*, vol. 15, no. 11, pp. 824–834, 2000.
[32] J. Sundell, "On the history of indoor air quality and health," *Indoor air*, vol. 14 Suppl 7, pp. 51–58, 2004.
[33] R. FLETCHER and B. JONSON, "DEADSPACE AND THE SINGLE BREATH TEST FOR CARBON DIOXIDE DURING ANAESTHESIA AND ARTIFICIAL VENTILATION: Effects of tidal volume and frequency of respiration," *British Journal of Anaesthesia*, vol. 56, no. 2, pp. 109–119, Feb. 1984.
[34] J. Glos, "FMUtoolbox for MATLAB/Simulink," in *22nd Conference STUDENT EEICT 2016*. Brno: Vysoké učení technické v Brně, Fakulta elektrotechniky a komunikačních technologií, 2016, pp. 426–430.
[35] L. Grüne and J. Pannek, *Nonlinear Model Predictive Control*, ser. Communications and Control Engineering. London: Springer London, 2011.
[36] M. A. Stephens, C. Manzie, and M. C. Good, "Model predictive control for reference tracking on an industrial machine tool servo drive," *IEEE Transactions on Industrial Informatics*, vol. 9, no. 2, pp. 808–816, 2013.
[37] D. Ariens, B. Houska, H. Ferreau, and F. Logist, "ACADO: Toolkit for Automatic Control and Dynamic Optimization," Optimization in Engineering Center (OPTEC), http://www.acadotoolkit.org/.
[38] H. Bock and K. Plitt, "A Multiple Shooting Algorithm for Direct Solution of Optimal Control Problems," *IFAC Proceedings Volumes*, vol. 17, no. 2, pp. 1603–1608, Jul. 1984.
[39] H. J. Ferreau, C. Kirches, A. Potschka, H. G. Bock, and M. Diehl, "qpOASES: A parametric active-set algorithm for quadratic programming," *Mathematical Programming Computation*, vol. 6, no. 4, pp. 327–363, 2014.
[40] H. J. Ferreau, H. G. Bock, and M. Diehl, "An online active set strategy to overcome the limitations of explicit MPC," *International Journal of Robust and Nonlinear Control*, vol. 18, no. 8, pp. 816–830, May 2008.
[41] G. Welch and G. Bishop, "An Introduction to the Kalman Filter," University of North Carolina at Chapel Hill, Tech. Rep., 1995.

Jan Glos received an M.Sc. and a Ph.D. degree in Cybernetics from Brno University of Technology, Brno, Czech Republic, in 2015 and 2020, respectively.

His current research interests include dynamic system modelling and simulation and application of advanced control algorithms in the field of heating, ventilation, air conditioning and refrigeration.

Lukáš Otava received an M.Sc. degree in Electrical Engineering from Brno University of Technology, Brno, Czech Republic, in 2013. He is currently working towards a Ph.D. degree in the field of fault detection for permanent magnet synchronous motors.

His current areas of research interest are permanent magnet synchronous motor drives for electric vehicles, and the implementation of control systems in an embedded multicore processor environment.

Pavel Václavek (M'04–SM'12) received an M.Sc. and a Ph.D. degree in Cybernetics from Brno University of Technology, Brno, Czech Republic, in 1993 and 2001, respectively, where he also received an M.Sc. degree in Industrial Management in 1998.

His research interests include speed-sensorless control of induction machines, system modelling, and parameters estimation. He is a Research Group Leader with the Central European Institute of Technology, Brno University of Technology.